Journal of the European Ceramic Society 19 (1999) 165–173

PII: S0955-2219(98)00187-3
0955-2219/98/$—see front matter

Fabrication of Pure YBaCuO Powders with Controlled Microstructure

C. Legros,[a]* C. Haut,[b] L. Ponsonnet-Mora[c] and J. Ayache[d]

[a]Laboratoire d'Etude des Matériaux Hors Equilibre (LEMHE), Université de Paris-Sud, Bât. 410, 91405 Orsay Cedex, France
[b]Laboratoire de Métallurgie Structurale, CNRS URA 1107, Université de Paris-Sud, Bât. 410, 91405 Orsay Cedex, France
[c]Laboratoire de Tribologie et Dynamique des Systèmes, Ecole Centrale de Lyon, CNRS UMR 5513, BP 163, 69131 Ecully, France
[d]CSNSM-IN2P3-CNRS, Bât. 108, Université de Paris-Sud, 91405 Orsay Cedex, France

(Received 23 January 1998; accepted 31 July 1998)

Abstract

A fabrication process has been optimized to successfully produce fine and pure high temperature superconducting YBaCuO powders. The resulting powders have been examined by X-ray diffraction, scanning and transmission electron microscopy with Energy Dispersive X-ray (EDXS) and Electron Energy Loss (EELS) Spectroscopies. Results show that this process allows the preparation of samples with a correct stoichiometry and a controlled microstructure without detectable secondary phases at grain boundaries to the scale of the transmission microscopy. A comparison of the powder quality is made with powders prepared by conventional methods.

Keywords: oxide superconductors, powders, solid state reaction, superconductivity, YBaCuO, chemical preparation.

1 Introduction

$YBa_2Cu_3O_{7-x}$ (noted 123 in the following) is one of the most extensively studied high-T_c superconductors. Nevertheless the control of its preparation is always a key point for obtaining suitable physical properties. For most technological applications, a high critical current density is required in the presence of high magnetic fields. This property is strongly dependent upon the microstructure achieved during the bulk processing. Controlling chemical composition at grain boundaries as well as the inter- or intra-granular secondary phases is a step of the utmost importance to obtain high-performance materials.

The preparation route for 123-powder most frequently reported in the literature is a solid-state diffusion reaction starting with Y_2O_3, CuO and $BaCO_3$ under a wide range of processing conditions. In this case, the decomposition of $BaCO_3$ appears to be the rate-limiting step. The calcination temperature must be high enough to obtain a significant decomposition rate of the carbonate. Generally, the powder is coarse with primary particles of about 10 μm, which form agglomerates of about 100 μm. The growth of primary particles and agglomerates increases with calcination temperature due to sintering effects. But for ceramic processing, a fine powder is required with a primary particle size of a few micrometer at most, preferably below 1 μm. Other powder synthesis methods which have been used for the preparation of superconductor are solution routes, more controllable and reproducible with improvement in purity and homogeneity. Such methods include coprecipitation (hydroxydes, oxalates, nitrates),[1,2] sol-gel method,[3,4] alkoxyde-hydrolysis,[5] spray and freeze-drying techniques.[6] There are also some disadvantages to these methods. For example, coprecipitation involves the use of precipitating agents which may remain in small quantities in the powder. Moreover, coprecipitation may not be uniform or complete in the case of a complex system such as YBaCuO, whose components have markedly different chemicophysical characteristics. Many of the above quoted methods lead to non-stoichiometry powder and their microstructure show the presence

*To whom correspondence should be addressed.

of secondary phases such as $BaCuO_2$ (011 phase) and Y_2BaCuO_5 (211 phase). Vapour-phase routes, such as chemical vapour deposition (CVD), molecular beam epitaxy (MBE)... are also able to provide selective, high-purity deposition of nanoparticles, but they suffer from the high cost of devices.

In an earlier study,[7] a synthesis procedure of the Co-, Ni- and Zn-substituted YBaCu-oxides, obtained through a modified nitrate route, has been shortly presented. Nitrates have been chosen because they have relatively low decomposition temperatures, and in contrast to oxalates or citrates, they cannot introduce carbonate or eventually carbon impurities which are undesirable for the sintering properties of the resulting powder. But characterization of the powders has shown that they were formed by fine ($\approx 1\,\mu$m) and homogeneous grains with an open porosity. Although chemical composition of powders was almost uniform throughout the samples, deficiency in copper was observed.

In this study, we present an elaboration process to produce very pure and homogeneous superconducting $YBa_2Cu_3O_{7-x}$ (our reference compound for the study of substituted ceramics). Each step of the synthesis procedure has been controlled, i.e. in optimizating processing parameters (temperature, time,...) and carrying out a characterization of the powder (phase purity, homogeneous microstructure, stoichiometric composition...). Results of transmission electron microscope (TEM) and microanalysis techniques: EDXS (Energy Dispersive X-ray Spectroscopy) and EELS (Electron Energy Loss Spectroscopy) are used for YBaCuO microstructure characterization.

2 Experimental

2.1 Powder elaboration

The procedure for elaborating pure YBCO powder is illustrated in the flowchart in Fig. 1. The process is based upon a modified nitrate route. Stoichiometric amounts of Y_2O_3 (Aldrich, no. EZ05519MV), $Ba(NO_3)_2$ (Aldrich, no. MX06610DW) and CuO (Aldrich, no. 75346) with purity ranging from 99 + % to 99·999% have been used to prepare a 25 g batch of 123. Powders are placed in concentrated (68% min) nitric acid and distilled water is added while stirring the mixture, until the nitrate solution becomes clear. The solution is then concentrated with a Büchi rotary evaporator, care has been taken to avoid a premature decomposition of the formed nitrates. The dried light blue nitrates mixture is then blended in diethyl oxide and sonificated with a Prolabo T275 Transsonic apparatus (35 Hz, 2·75 L, 285 W) for 1 h 30 min. After excess

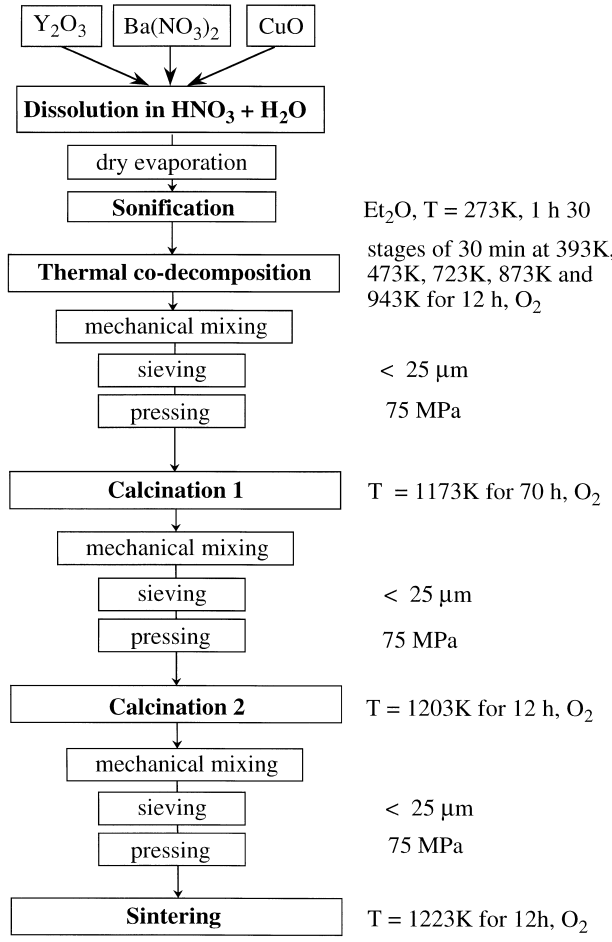

Fig. 1. Flowchart for chemical processing of $YBa_2Cu_3O_7$.

Et_2O is removed, the nitrate mixture is placed in an alumina crucible to be decomposed. The decomposition is carried out by stages of 30 min respectively at 393, 473, 723, 873 K and finally the furnace is set to 943 K for 12 h. The product is then mixed in a 250 ml polyethylene jar containing ZrO_2 balls ($\Phi = 4$ mm) in a 2-propanol medium for 2 h, for desagglomeration purpose and to reduce grain size. After filtration, drying and sieving at $\leq 20\,\mu$m, the mixture is uniaxially pressed (75 MPa) into pellet form and calcined at 1173 K for 70 h. The pellet is then reground, resieved in the same conditions and calcined at 1203 K for 12 h, and finally sintered at 1223 K for 12 h with an intermediate mechanically grinding and sieving. All these thermal treatments take place with a heating rate of 3 K min^{-1}, a cooling rate of 5 K min^{-1} and under a flowing oxygen atmosphere. In order to allow a maximum oxygen uptake, the last sintering is followed by (i) a slow cooling from 1223 K, (ii) temperature plateaus between 773 and 573 K, (iii) temperature plateau at 573 K for several days, (iv) cooling down to room temperature.

2.2 Characterization

The powder phase purity is characterized by X-ray diffraction (XRD) at various stages of the processing.

The XRD equipment consisted of a Philips PW 3020 diffractometer with nickel-filtered CuK_α radiation. Data are collected while scanning the rotating sample at $1° \text{ min}^{-1}$ (2θ) and a step size of 0·02° (2θ) Checking the product only by this type of scan, named standard scan, is inadequate to detect the presence of secondary phases such as $BaCuO_2$, Y_2BaCuO_5, Y_2CuO_5 ... [Fig. 2(a)]. Consequently, a more sensitive scan (named slow scan) for detecting traces of these secondary phases has been developed for this work. XRD patterns are scanned step by step with a step size of 0·005° (2θ) and a time per step of 50 s in the 27–32° (2θ) range, interval where these phases can be easily detected [Fig. 2(b)].

Microstructural observations on fractured surfaces are carried out using a LEICA 260 scanning electron microscope (SEM) equipped with a Tracor Noran Energy-Dispersive X-ray spectrometer. On various selected areas, the quantitative elemental analysis is performed using the matrix correction program ZAF.

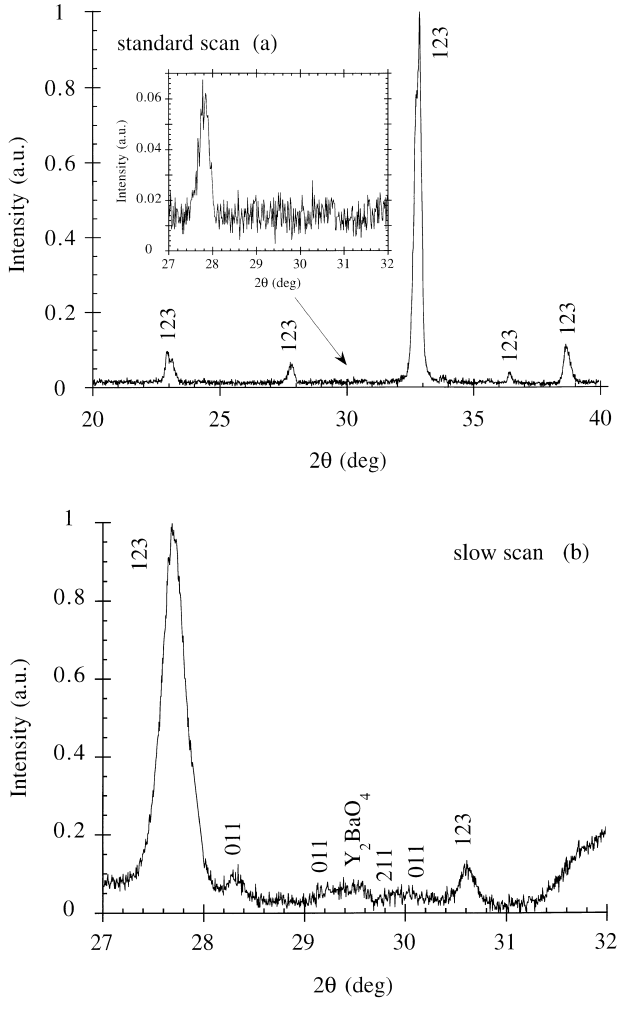

Fig. 2. Powder X-ray diffraction patterns using CuK_α radiation for a sample annealed to 1203 K for 12 h in O_2: (a) standard scan where secondary phases are not detected, (b) slow scan where phases such as 011, 211 and Y_2BaO_4 are detected.

Some samples have been also examined by scanning transmission electron microscopy (STEM). The quantitative microanalysis has been investigated by two different analytical microscopy techniques: EDXS and PEELS.

EDXS analyses have been performed with a Tracor Noran Energy Dispersive X-ray spectrometer on a JEOL 2000 EX TEM equipped with a LaB_6 filament operating at 200 kV. Samples for EDX are prepared by the tripod polisher method described in reference.[8] This method has been preferred to the standard method of polishing using ion milling. This TEM sample preparation allows to avoid any extrinsic defect formation due to ion milling. It produces better specimens with a better chemical stability and with controlled thickness. These features are of great importance especially for the study of the variations of chemical stoichiometry, which is the case in this work. Specimens are placed between two holey carbon-filmed aluminium grids in order to get access to the four elements analysis. EDXS chemical analysis is carried out on various selected thin primary particles and care has been taken to control the stoichiometry through grain boundaries.

High quality electron energy loss spectra have been obtained using the EL/P Gatan software fitted with a parallel recording system attached to a TEM. PEELS analysis have been performed with a Gatan Model 666 spectrometer on a Philips EM 420 TEM also equipped with a LaB_6 filament operating at 120 kV. Samples have been embedded with an epoxy resin of a high beam stability (Embed 812 Epon) and microtomed at room temperature on a LKB 2188 Ultratome (NOVA) according to the experimental procedure described in reference 9. To be analysed, thin foils have been deposited on top of copper grids covered with holey carbon. The microscope operates in the diffraction mode configuration in order to obtain a high signal/noise ratio. The width of the zero loss peak was typically 1·5 eV fwhm, this latter representing the resolution of the experiments. Numerous areas have been explored to determine only the barium and oxygen stoichiometries. The copper stoichiometry cannot be analysed because of the nature of the grids.

Sintering test has been performed in a differential dilatometer SETARAM DHT under oxygen flow, with a constant heating rate of 3 K min^{-1} up to 1238 K. Sapphire plates have been used as a barrier between the sample and alumina sensor rod on top and the sample holder at the bottom to avoid interaction between alumina and 123. The length change is continuously in situ measured and the results are plotted as curves of shrinkage and shrinkage rate versus temperature.

3 Results and discussion

3.1 Powder elaboration

Let us investigate in more details the procedure presented in Fig. 1. The originality of the process lies in the sonically treatment which the nitrates mixture undergoes in Et_2O. By this operation, the powder is disagglomerated, the particle size is reduced and their reactivity increased in order to ensure an optimum thermal co-decomposition of nitrate salts. Thus, chemical homogeneity is improved in final and density of the end product is increased. The thermal behaviour of the nitrates salts of Y, Ba and Cu was studied long time ago. Wendlandt[10] has established that $Y(NO_3)_3$, $6H_2O$ begins to lose water at room temperature and with increasing temperature an oxynitrate $YONO_3$ is formed at 713–748 K, which decomposes completely to Y_2O_3 at 933 K. According to Gordon *et al.*[11], $Ba(NO_3)_2$ and $Cu(NO_3)_2$ decompose in two steps as follows:

$$Ba(NO_3)_2 \xrightarrow{861\ K} Ba(NO_2)_2 + O_2$$

$$Ba(NO_2)_2 \xrightarrow{873\ K} BaO + NO + NO_3$$

$$Cu(NO_3)_2 \xrightarrow{393\ K} Cu(NO_2)_2 + O_2$$

$$Cu(NO_2)_2 \xrightarrow{473\ K} CuO + NO + NO_3$$

Knowing these temperatures and in order to avoid explosion, the co-decomposition has been performed in an oxygen flow by stages at 393, 473, 723, 873 K, each temperature corresponding approximately to one step of decomposition of a nitrate salt. Finally, the temperature is raised to 943 K during a long time enough. It is necessary to maintain the furnace at this temperature during 12 h to ensure the complete decomposition; with a lower time, powder still includes $Ba(NO_3)_2$. After decomposition, XRD analysis in standard scanning showed that the powder is composed of three phases: CuO, Y_2O_3 ans $Ba_2Cu_3O_{5\cdot9}$. As soon as $Ba(NO_3)_2$ decomposes, it reacts with CuO to form $Ba_2Cu_3O_{5\cdot9}$. The SEM micrograph of a fractured surface reveals large agglomerates of irregular grains of different shape. This stage of the process is very important because what follows is determined by the repartition of the various phases in the material and their reactivity. The reactivity is particularly dependent of the grain size of particles.

The calcination temperature of 1173 K has been chosen according to the earlier study[7] where it has been shown that the superconducting phase began to form at a temperature of about 1073 K, and that the content of superconducting phase for the 1173 K-treated sample is higher than that for the 1073 K-treated sample. XRD standard pattern of sample calcined at 1173 K is not given here but the main X-ray diffraction lines belong to the superconducting phase, but nonsuperconducting phases, mainly $BaCuO_2$ and Y_2BaCuO_5 can be also detected. The microstructure of this sample which is shown in Fig. 3(a) exhibits a very bad sintered material of heterogeneous composition. Grain size is also very inhomogeneous and the porosity is enormous despite a long time treatment (70 h). Due to this porosity, the grains of different phases do not show a common interface. As a consequence, the solid state diffusion cannot be operative to achieve chemical compositional homogeneity. Therefore, it is necessary to carry on the powder processing to get a better chemical homogeneity. For the second calcination, the temperature has been chosen in accordance with sintering behaviour of a powder compact studied by dilatometry.

Typical shrinkage curve and densification rate curve are plotted in Fig. 4 for sintering in oxygen. This sintering behaviour is quite different from those reported in the literature.[12,13] In these cases, a small shrinkage up to $T \leq 1173$ K caused by the decomposition of $BaCO_3$ and a drastic acceleration of the sintering at $T \approx 1193$ K, due to the occurrence of a liquid phase, were revealed. In our case, up to $T < 1173$ K, no shrinkage is observed. The shrinkage occurs in two steps over an extremely narrow temperature range [1183–1223 K]. The densification starts at ≈ 1183 K, going rise to a first peak at 1203 K followed by a second one at 1223 K. All these observations are consistent with a solid phase sintering process followed by a liquid phase sintering one. It will be shown later on that the liquid phase is provided by secondary phases. After sintering at 1203 K, 12 h in oxygen flow, porosity is once again too high to allow solid state diffusion as can be seen in Fig. 3(b). Chemical homogenization is then not complete, main diffraction lines of remaining secondary phases were yet detected but only in the slow scan. After sintering at 1223 K, high-quality 123 material with a 85% relative density is obtained.

Comparison of our results has been done with those found in the literature i.e. (i) a powder prepared by the conventional solid state reaction optimized by Lanckbeen *et al.*[14], (ii) a commercial Hœchst powder obtained via a nitrate route (impurities $< 2{\cdot}10^{-3}$ mass fraction, parasite phases $< 5{\cdot}10^{-3}$ mass fraction), (iii) a powder prepared at C.R.P.H.T. (Orléans) by firing a commercial Hœscht powder, in an oxygen atmosphere at increasing temperatures (1188–1218 K) for 8 h with

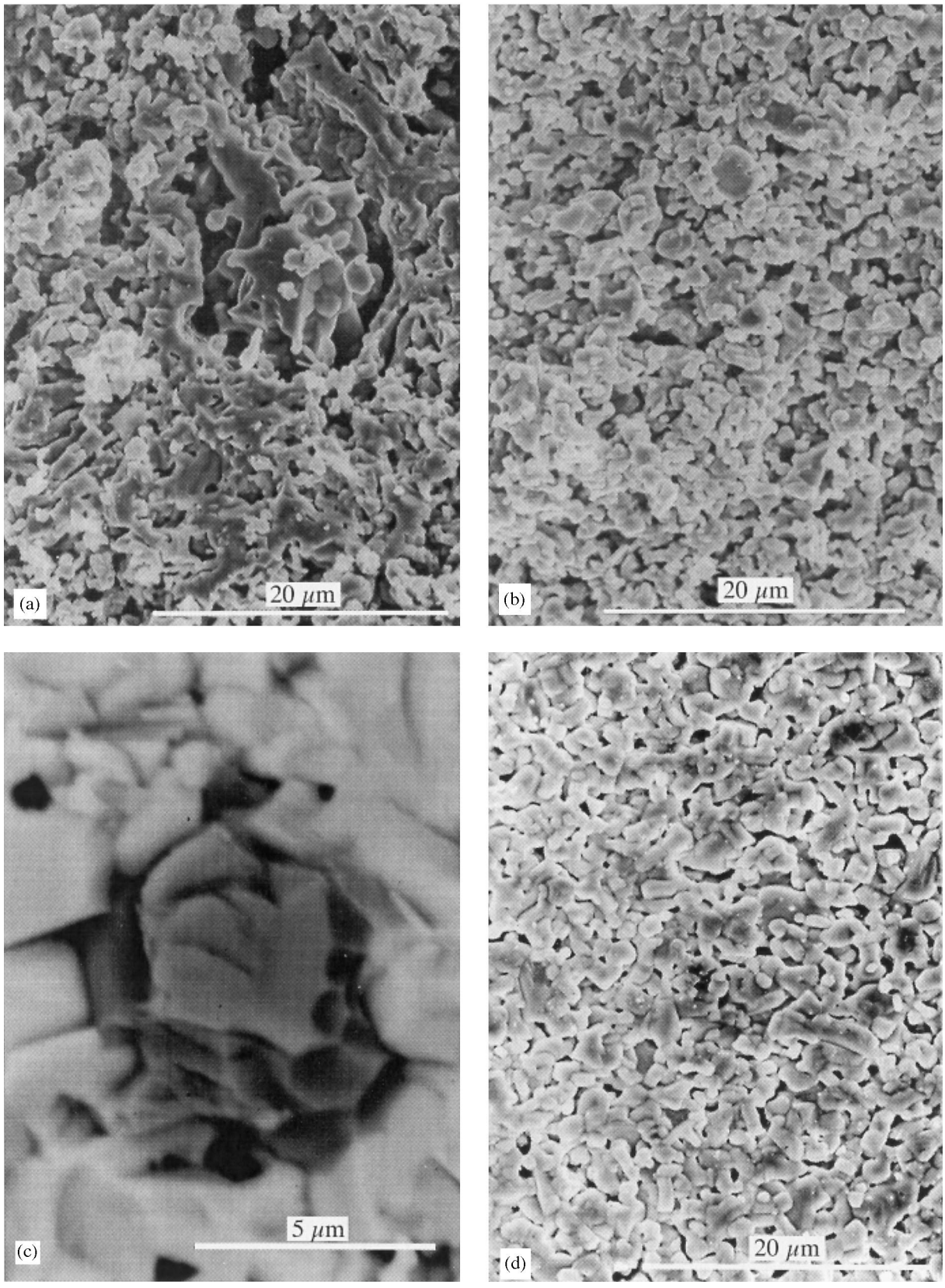

Fig. 3. SEM micrographs of fractured surfaces of (a) sample after calcination 1 to 1173 K for 70 h under O_2, (b) sample after calcination 2–1203 K for 12 h under O_2, (c) sample after sintering to 1223 K for 96 h under O_2, (d) sample of sintering to 1223 K for 12 h under O_2.

intermediate grindings in order to minimize the quantity of secondary phases. Figure 5 shows the different comparative X-ray diffraction patterns using the slow scan described in section 2·2. Great differences can be observed. Secondary phases remain in the oxide for these three samples, only our powder is cleaned at high resolution detection.

For sintering at 1223 K, it is important to control the rate of liquid phase formation by properly adjusting the sintering profile. If the rate is too fast,

grain growth is reduced and porosity remained important. So, when the temperature reaches 1223 K, although liquid phase forms, it is in too small proportions to wet all grains of '123' and realize chemical homogeneity. With a sintering rate of 3 K min^{-1} and adapting the time of thermal treatment, it is possible to reach homogeneity. Indeed, we have shown that this time generates a critical grain size controlling the quality of the powder. Holding the sample 12 h at 1223 K with a sintering rate of 3 K min^{-1} represents the best conditions: if time is shorter, grain size is still too small to allow solid state diffusion and chemical homogenization, and with prolongated time, grain growth is observed but the grain size becomes too large to homogenize local deviations from stoichiometry and secondary phases segregated at the growth front leading to an inhomogeneous microstructure as shown in Fig. 3(c).

Then, the most significant improvements made with this elaboration route concern the secondary phases disposal.

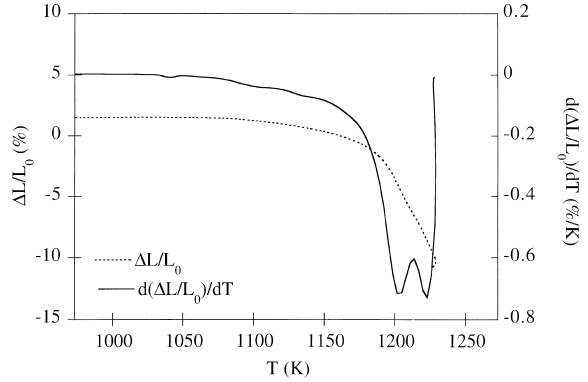

Fig. 4. Shrinkage and differential shrinkage curves versus T during sintering at a heating rate of 3 K min^{-1} for powder compact of 123.

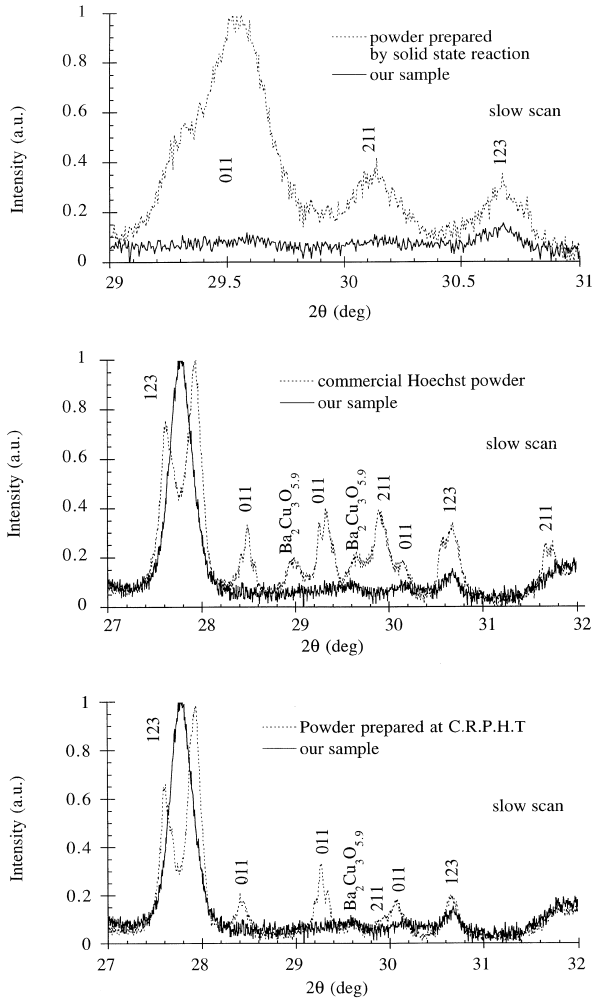

Fig. 5. Comparative powder X-ray diffraction patterns using slow scan between our sample after sintering to 1223 K for 12 h under oxygen and: (a) powder prepared by the conventional solid state reaction, (b) a commercial Hœchst powder obtained through a nitrate route, (c) a powder prepared at C.R.P.H.T. (Orléans, France) after annealings of the commercial Hœchst powder at increasing temperatures (1188–1218 K) in an oxygen atmosphere.

3.2 Microstructural and chemical analysis characterization

3.2.1 Microstructural results

Figure 3(d) presents a scanning electron micrograph at 20 kV of a pellet sintered at 1223 K for 12 h in oxygen. This photomicrograph shows that the superconducting ceramic was formed by very fine ($\approx 1\,\mu$m) and homogeneous grain size with an open porosity.

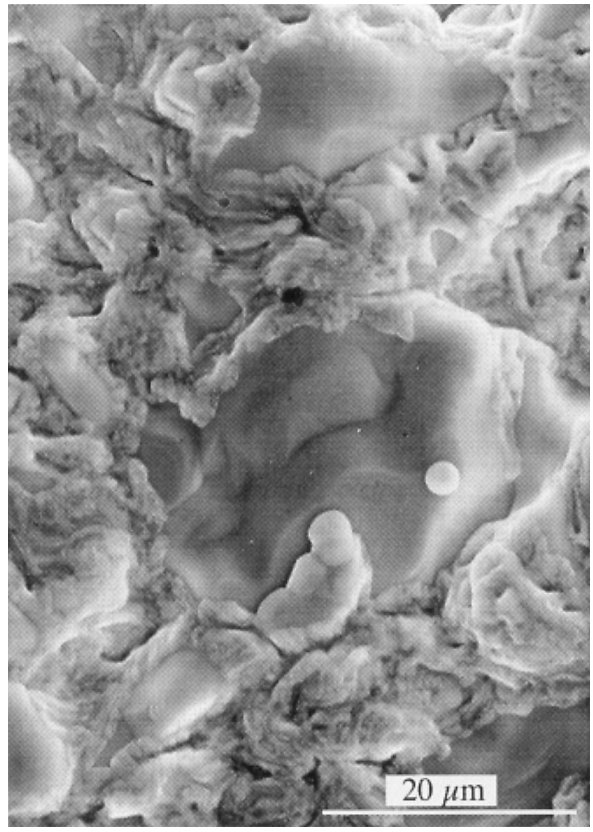

Fig. 6. SEM micrograph of fractured surface of a sample prepared by the conventional solid state reaction.

Figure 6 illustrates for comparison, a SEM micrograph of a sintered sample prepared by the classical solid state heat treatment as described in Marucco and Glé.[15] For a better understanding, a short presentation of its preparation is recalled. Appropriate amounts of high purity powder of Y_2O_3, $BaCO_3$ and CuO were thoroughly mixed in an agate mortar, pressed into pellets and annealed several times (with intermediate manual grinding) at 1213 K under oxygen flowing. Great differences can be observed in grain size, homogeneity and porosity.

Figure 7(a) exhibits a typical TEM micrograph of a thin foil of the sample sintered at 1223 K for 12 h in oxygen flow. The arrows point out the different grain boundaries. This picture shows evidence of clean grain boundaries. At the scale of detection of TEM, no secondary phase was detected at grain boundaries as can also be seen in Fig. 7(b). Moreover, twins observed in Fig. 7(c) indicate the presence of the orthorhombic phase.

3.2.2 Chemical analysis results

Elemental analysis by EDXS of a number of particles of the sample, presented in Fig. 3(d), indicates a homogeneous composition of Y, Ba, Cu with no variation (within experimental error) in composition from one grain to another throughout the sample. This analysis is just indicative because it has been carried out only a fractured surface, not a polished one.

X-ray elemental analysis at the scale of TEM also indicates that the sample is very homogeneous with no variation in composition of Y ($7{\cdot}43 \pm 0{\cdot}42$),

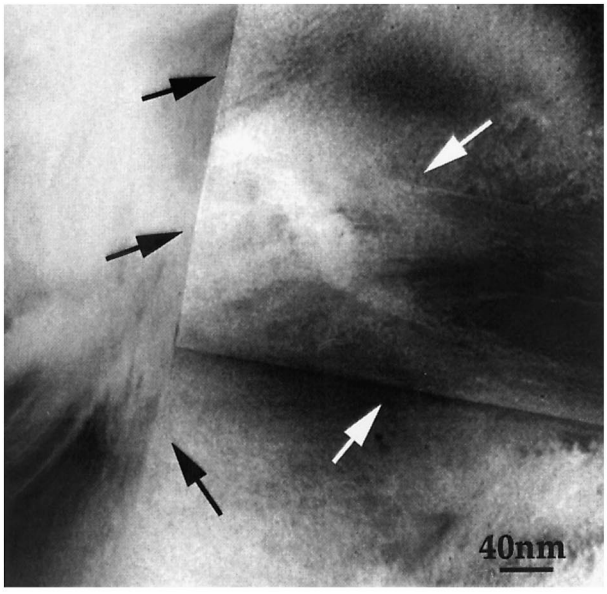

(a)

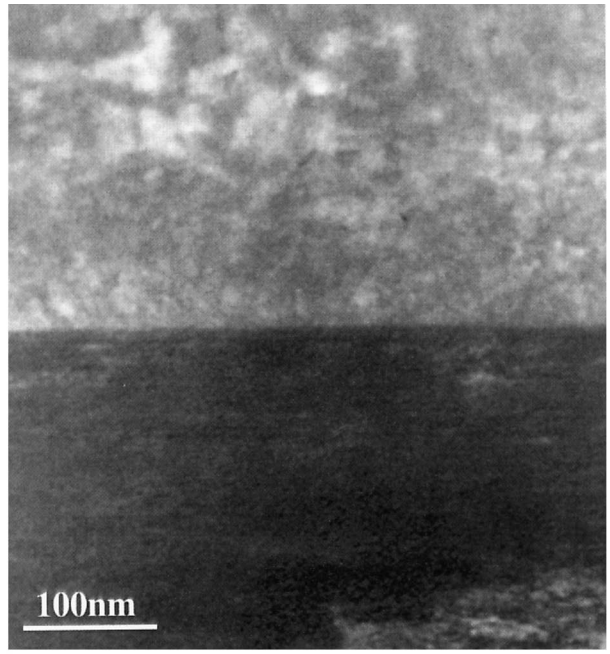

(b)

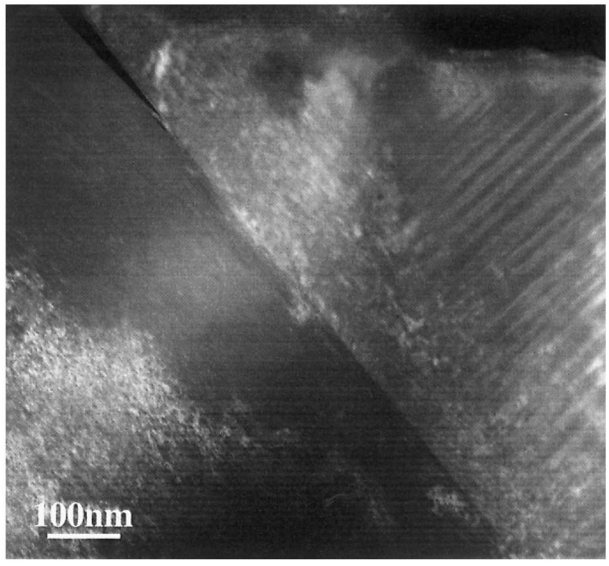

(c)

Fig. 7. (a) STEM micrograph of our sample after sintering to 1223 K for 12 h under oxygen, (b) presents a grain boundary without secondary phases and (c) shows the twin structure.

Ba(14·94 ± 0·84), Cu (22·73 ± 2·03) across the sample and through the grain boundaries.

EELS quantitative microanalysis has been realized on this sample. This quantitative method is based on the fact that the ratio of the core-loss peak intensifies arising from the different elements (A and B) is proportional to their local atomic ratio. Therefore, changes in chemical composition can be revealed by the variation of the ratios issued from quantification. Quantification of the signals, issued from the ionization edge intensities in the spectrum, implies the use of appropriate standard ionization edge for each chemical element and also background corrections. A cold-stage specimen holder was used to lower the specimen temperature to 92 K to minimize sample contamination and beam damage. Indeed, it is known that the oxygen K-edge spectrum is modified with increasing electron beam irradiation.[16] As it has been shown by Nucker *et al.*,[17] the intensity of the O–K edge peak is related to the oxygen stoichiometry in 123. Thus, in our experiments, in order to limit beam damages during the acquisition of the spectra, the minimum acquisition time to obtain a good signal to noise ratio, typically 0·8 s has been taken. The spectrum in Fig. 8 shows the edge features of the O–K, Ba–M_4 and Cu–L_3 edges for a sample heated to 1223 K for 12 h in O_2. The quantification of this spectrum gives a value of the atomic ratio: Ba/O = 0·29 and Cu/O = 0·38. Different areas have been analysed and have brought to the same values (5% incertainty). As referring to theoretical values (Ba/O = 0·29 and Cu/O = 0·43), these results show clearly that the good stoichiometry is maintained during processing.

Comparative analysis has been investigated on the sample prepared by the conventional solid state reaction and is shown in Fig. 6. EDXS analysis indicates a large variation from one grain to another and STEM studies reveals that the sample consists mostly of twin-orthorhombic $YBa_2Cu_3O_{7-x}$ phase, running all across the sample with very few other phases detected. PEELS microanalysis has been also checked. Same kind of quantitative analysis has been performed in the same experimental conditions than for the previous sample. It can be noted that the dispersion in the results when changing the area of interest is large: Ba/O = 0·25 and Cu/O = 0·15–0·5 with an average value of 0·27. Consequently, it can be said that our sample if of higher quality.

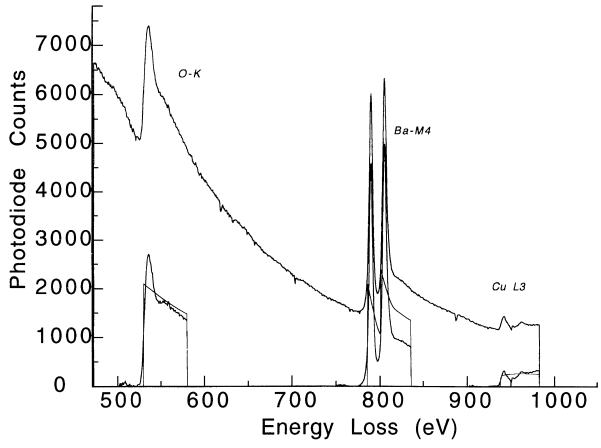

Fig. 8. EELS spectrum of our sample after sintering to 1223 K for 12 h under oxygen for O-K, Ba-M_4 and Cu-L_3 edges.

4 Conclusions

A detailed study on the elaboration and the concomitant structural and microstructural evolution of the YBaCu-oxide system has been carried out. Elaboration was investigated through a modified nitrate route. The advantage of the procedure developed here lies in sonification of the mixture nitrates which allows to increase the reactivity of the particles and to improve the final chemical homogeneity. Then, by controlling the critical steps, it is possible to prepare in a reproducible way fine and high-purity powders by sintering at 1223 K in flowing oxygen during 12 h. Further research is in progress to prove their superconducting behaviour which will be reported elsewhere.

This method has been also applied to produce for the first time single phase material of $Y_{1-x}Ce_xBa_2BiO_6$ ($0 \leq x \leq 1$) although by solid state chemistry, powders include two different phases YBa_2BiO_6 and $CeBa_2BiO_6$ for $x \leq 0{\cdot}2$. Consequently this method can be extended to prepare other oxide powders.

Acknowledgements

The authors are very grateful to Pr. C. P. Carry for valuable discussions, Dr. M. Demartin for dilatometric measurements, Dr. C. Picard for providing the two samples of Hœchst commercial powder and J. Tribout for experimental contribution.

References

1. Barboux, P., Campion, I., Daglish, S., Livage, J., Genicon, J. L., Sulpice, A. and Tournier, R., Synthesis of $YBa_2Cu_3O_{6+x}$ from coprecipitated hydroxydes. *J. Non Cryst. Sol.*, 1992, **147–148**, 720.
2. Kumar, P., Pillai, V. and Shah, D. O., Preparation of $YBa_2Cu_3O_{7-x}$ superconductor by oxalate coprecipitation. *J. Mater. Sci. Lett.*, 1993, **12**(3), 162–164.
3. Aoki, A., Ohno, S. and Muramatsu, Y., *J. Non Cryst. Sol.* 1992, **147–148** 704.
4. Nishio, T. and Fujiki, Y., Preparation of superconducting $YBa_2Cu_3O_{7-x}$ fibres through metal citrate gel as a precursor. *J. Mater. Sci. Lett.*, 1993, **12**(6), 394–398.

5. Pak, S. S., Montgomery, F. C., Duggan, D. M., Chen, K. C., Mazdiyasni, K. S., Tasi, P. K., Paulius, M. and Maple, M. B., Solution condensed $YBa_2Cu_3O_{7-x}$ superconductor thin films from setting metal-organic precursors. *J. Amer. Ceram. Soc.*, 1992, **75**(8), 2268–2275.
6. Coppa, N. V., Myer, G. H., Salomon, R. E., Bura, A., O'Reilly, J. W., Crow, J. E. and Davies, P. K., Preparation, thermal processing behavior, and characterization of YBCO from freeze-dried nitrate precursors. *J. Mater. Res.*, 1992, **7**(8), 2017–2026.
7. Legros, C., Fortin, S. and Marucco, J. F., Synthesis of pure and fine Co, Ni and Zn-doped YBaCuO powders. *Physica C*, 1994, **235–240**, 799–800.
8. Ayache, J. and Albarède, P. H., Application of the ionless tripod polisher to the preparation of YBCO superconducting multilayer and bulk ceramics thin films. *Ultramicroscopy*, 1995, **60**, 195–206.
9. Birken, I., Thesis, Caractérisation de catalyseurs de fluoration par spectroscopie d'absorption X et spectroscopie de perte d'énergie des électrons transmis. Ecole Centrale de Lyon, 21 juin 1996, Lyon, France.
10. Wendlandt, W. W., The thermolysis of rare earth and other nitrates. *Anal. Chim. Acta*, 1956, **15**, 435–439.
11. Gordon, S. and Campbell, C., Differential thermal analysis of inorganic compounds. *Anal. Chem.*, 1955, **27**, 1102–1109.
12. Odier, P., Dubois, B., Gervais, M. and Douy, A., Chemical inhomogeneities in YBaCuO procudes by conventional sintering. *Mater. Res. Bull.*, 1989, **24**, 11–22.
13. Greuter, T., Kluge-Weiss, P., Zimmermann, H. and Schuler, C., Preparation and microstructure of high density $Y_1Ba_2Cu_3O_{7-\delta}$. *Physica C*, 1988, **153–155**, 361–362.
14. Lanckbeen, A., Duvignaud, P. H., Diko, P., Mehbod, M., Naessen, C. and Deltour, R., Effect of zinc and iron on the (micro-)structure and copper charge excess of the YBaCuO superconductor. *J. Mater. Sci.*, 1994, **29**, 5441–5447.
15. Marucco, J.-F. and Glédel, C., Non-stoichiometry and thermodynamics of defects in the system YBa_2Cu_3O. *Physica C*, 1989, **160**, 73–79.
16. Browning, N. D., Yuan, J. and Brown, L. M., Quantification of spatial fluctuations of oxygen stoichiometry in $YBa_2Cu_3O_{7-\delta}$. *Supercond. Sci. Technol.*, 1991, **4**, 346–348.
17. Nücker, N., Fink, J., Fuggle, J. C., Durham, P. J. and Temmerman, W. M., Evidence for holes on oxygen sites in the high-T_c superconductors $La_{2-x}Sr_xCuO_4$ and $YBa_2Cu_3O_{7-y}$. *Phys. Rev. B*, 1988, **37**, 5158–5163.